Adsorption 9: 37–54, 2003

Frequency Response Method for Measuring Mass Transfer Rates in Adsorbents via Pressure Perturbation*

BRIAN K. SWARD AND M. DOUGLAS LEVAN**
Department of Chemical Engineering, Vanderbilt University, VU Station B 351604, Nashville, Tennessee 37235, USA

Received January 16, 2002; Revised July 18, 2002; Accepted August 14, 2002

Abstract. A new apparatus for the measurement of equilibria and dynamics for gas-phase adsorption systems is utilized to examine the adsorption of carbon dioxide on BPL activated carbon. The apparatus has a flow-through configuration. For dynamics, with constant inlet flow, pressure within the adsorbent-containing section is varied sinusoidally, and the time-dependent outlet flow rate is measured to determine an amplitude ratio and phase lag. Studies are made of temperature effects and particle size effects. Results are compared with several mathematical models. Frequency response data show that the BPL system follows surface (or micropore) diffusion kinetics. The rate of adsorption for the activated carbon is found to be only weakly dependent on the bulk particle size.

Keywords: frequence response, surface diffusion, micropore diffusion, dynamics, rate, kinetics

Introduction

The characterization of adsorption dynamics is necessary in order to design many systems accurately. The two most common ways of obtaining adsorption properties are through gravimetric uptake and volumetric measurements. Both of these techniques have their limitations for measuring dynamics. They both require step changes in the concentration of the sample which are generally large. Allowance for heat effects can be complex.

Frequency response is a perturbation method in which some property of a system is varied periodically about an equilibrium state. The responses of system variables to the variation are used to characterize the system. By perturbing the system about an equilibrium state, the potential for experimental error during the initial contact stage in the step change methods is reduced (Grzegorczyk and Carta, 1997). It is possible in many instances to discriminate between various mass transfer mechanisms by examining the response over a large frequency spectrum (Jordi and Do, 1993). In addition, frequency response methods allow for the determination of system characteristics over much smaller changes in the system conditions than are typically used for the step change methods.

The most common method of studying adsorption dynamics by frequency response is periodically varying the system volume by a small amount, typically 1 to 2% of the total volume, and observing changes in the pressure within a closed system. This technique was first used by Polinski and Naphtali (1963). Yasuda and Yamamoto (1985) claimed to have shown the existence of two separate types of adsorbed species with differing mobilities in their study of light hydrocarbons on zeolite 5A. Van-Den-Begin et al. (1989) provide a comparison of results obtained for the diffusivity of ethane on silicalite as determined by frequency response, a step-change sorption uptake method, and by nuclear magnetic resonance (NMR). They found that the self-diffusion coefficients measured by two NMR techniques were approximately

*Presented in the Adsorption Symposium Honoring Shivaji Sircar at the AIChE 2001 Annual Meeting, Reno, Nevada, November 2001.
**To whom correspondence should be addressed.

150 times larger than the diffusion coefficients obtained from frequency response and step change methods. Onyestyak and Rees (1999) have used the frequency response method to study the mobilities of various adsorbates on different commercial adsorbents, leading to dynamical characterization of adsorbents in terms of rate mechanism.

Jordi and Do (1993) made an in-depth analysis of various mass transfer mechanisms in bidisperse adsorbents, and provided guidelines for their applicability to various frequency response systems. The study was then extended to non-isothermal systems including the influence of heat release on adsorption capacity and diffusion rates (Jordi and Do, 1994). Yasuda (1994) and Bülow and Micke (1995) have published extensive review articles which emphasize the behavior of batch systems. The monographs of Kärger and Ruthven (1992) and Do (1998) also provide excellent coverage.

Sun et al. (1993a) showed that in batch systems small perturbations in the system cannot eliminate temperature effects if they are present in a system. This is due to the fact that although the loading changes caused by the released heat of sorption are reduced, as the perturbations are decreased in magnitude, they scale at the same rate as the overall change in the loading of the system. Sun et al. (1993b) also showed that if heat effects are involved, the out-of-phase components of the frequency response may exhibit a bimodal response. They re-analyzed the data of Yasuda and Yamamoto (1985) and determined that heat effects were the cause of the bimodal response seen in the zeolite studies. In addition, they found that when both macroporous and microporous resistances were present, the macropore resistance acts like a surface barrier.

Bourdin et al. (1996) and Grenier et al. (1999) added measurement of the temperature response to the pressure response within a batch system to simultaneously determine heat and mass transfer resistances. They did so through the use of infrared measurement of the sample temperature. They found that the thermal relaxation of the gas was fast enough that one could assume that the gas phase temperature was constant and that heat transfer from the particle to the gas was the controlling heat transfer resistance.

While batch systems are in the majority, other techniques have been explored as well. Boniface and Ruthven (1985) varied the inlet concentration to a chromatographic column sinusoidally in an effort to determine axial diffusion coefficients, diffusivities within zeolites, and adsorption equilibrium data. Li et al. (1989) utilized a flow system and infrared spectroscopy to determine sticking coefficients for the chemisorption of carbon monoxide on a platinum catalyst. Grzegorczyk and Carta (1997) modulated the temperature of a liquid phase adsorption system to study the mass transfer of amino acids adsorbed on polymeric adsorbents.

Park et al. (1998a and 1998b) described an apparatus where the mass flow into the system is varied and the pressure response is measured. The system operates as either a semi-batch adsorber or a continuous flow adsorber. For continuous flow operation, a valve is used to allow a constant volumetric flow rate to exit the system. They described both a single bed system and a two bed system where the flow fed to the two beds is π out of phase and the differential pressure between the two beds is measured. Petkovska and Do (1998, 2000) expanded the analysis of this system to include nonlinear frequency response for isothermal systems. They found that using second order frequency response functions made it possible to more readily distinguish identity of the rate controlling mechanism. Simulated experimental data were used to demonstrate the analysis. Prasetyo and Do (1998) published data using a similar apparatus to the batch system described by Park et al. (1998a) using a constant molar flow rate at low pressures to measure the adsorption of methane and carbon dioxide on activated carbon.

Studies have shown that while it is often a good approximation, the linear driving force coefficient, when used to model surface diffusion, may change with the cycling time of a system. Nakao and Suzuki (1983) studied the effects of cycle frequency on the intraparticle distribution of adsorbate. They demonstrated that increasing the cycling frequency raised the effective linear driving force coefficient. Alpay and Scott (1991) used penetration theory to show that for very short cycle times the linear driving force was proportional to the square root of the the frequency. Carta (1992) provided another theoretical treatment of particle diffusivity allowing the prediction of the linear driving force coefficient over a wide range of frequencies.

This work describes a simple flow system where the pressure of the system is the controlled variable and the outlet flow rate of gas is the measured variable. A material balance on the open system is used to determine both frequency response and equilibrium characteristics for the adsorption of a gas. Both isothermal and non-isothermal linear driving force (LDF) and surface (micropore) diffusion models have been developed.

In addition, a multiple resistance linear driving force model has been developed as an example of a non-homogeneous pore size model.

Experimental Apparatus

The experimental apparatus for the flow system is shown in Fig. 1. It consists of a mass flow controller (MKS type 1179), an adsorbent bed, a pressure controller (MKS type 640A), and a mass flow meter (MKS type 179). Gas enters the system through the mass flow controller at a constant rate and passes through the adsorbent bed, the pressure controller, and the mass flow meter and then exits to vacuum. Valves and a bypass line around the bed are present to allow the use of the flow system for adsorption equilibrium measurements. The bypass line helps to eliminate pressure drops through the bed during frequency response experiments.

Some system specifications and capacities are as follows. The flow rate through the mass flow controller is adjustable from 0–10 sccm of N_2. The mass flow meter range is also 0–10 sccm N_2. Two different pressure controllers with pressure ranges of 0–1000 torr and 0–100 psi can easily be interchanged through the use of VCR fittings. The volume of the system between the mass flow controller and the pressure controller is about 60 cm^3, and the bed is capable of holding up to 9 g of activated carbon.

System control and data acquisition are achieved through the use of a National Instruments 6052E data acquisition card installed in a Dell Dimension XPS B1000r 1 GHz Pentium III computer running National Instruments LabView software. This system has the ability to sample data up to 290 times per second.

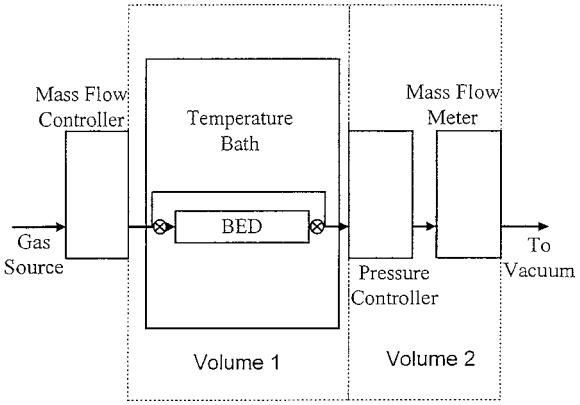

Figure 1. Apparatus.

Adsorption Equilibrium

To measure adsorption equilibrium, the valves to the bed are closed, isolating the bed from the system. Flow of the adsorbate is allowed to enter the system, bypassing the bed. The pressure controller is set to the desired pressure point and the system is allowed to come to initial steady values, at which time the mass flow in is equal to the mass flow out. The valves to the bed are then opened and the pressure and mass flow rate out both decrease. Data are recorded until the pressure and mass flow rate out are re-established at the initial steady values. The difference in the mass flow rates into and out of the bed is integrated over the length of the run to determine the total mass flows in and out of the bed. This is the amount of the component accumulated within the system in both the adsorbed and gas phases. The bed is then isolated again. A new pressure equilibrium is established and the measurement technique repeated.

The theory for adsorption equilibrium determination is based on a simple material balance for an isothermal system. If the gas is taken as ideal, for any given pressure change ΔP, the change in amount adsorbed is given by

$$M_b \Delta n = \int_0^t [F_{\text{in}} - F_{\text{out}}(\tau)]\, d\tau - \frac{V_f \Delta P}{RT} \qquad (1)$$

where M_b is the mass of the adsorbent, n is the amount adsorbed, t is the time required for the system to reach equilibrium, F is the molar flow rate, and V_f is the active volume of the system excluding the skeletal volume of the adsorbent. All heat effects can be neglected because the initial and final temperatures are the same.

Prior to measurements, the adsorbent bed was cleaned by heating the bed to 350 K and flowing helium through the bed for 24 hours at 1 cm^3/min (STP) while applying a vacuum, maintaining total system pressure at below 10 torr. Regeneration was verified by stopping the helium flow and measuring the minimum pressure reached.

When a non-adsorbable, inert component was necessary for determining system parameters, helium (99.999% purity) was used. We sought to measure any adsorption of helium at room temperature, determining it to be negligible.

The isotherm for carbon dioxide (99.8% purity bone dry grade) adsorbed on activated carbon was determined at 297 K over the range 1.2 kPa–482.6 kPa. The bed was filled with 3.25 g of activated carbon (Calgon BPL), which was regenerated as described above. (In additional measurements, the weights of the samples were determined by regenerating at 200°C for 12 hours with helium flowing at 1 l/min, and then weighing.) The low pressure limit of 1.2 kPa (9 torr) was determined by the minimum nonzero flowrate through the mass flow controller. The upper pressure was limited by the gas cylinder pressure regulator.

The apparatus made it possible to obtain the data quickly. Depending on the pressure change and the flow rates of gas used, the time for the system to reestablish stable flow was between 10 minutes and two hours, with only the lowest pressure points, which required the lowest flow rates, requiring more than 25 minutes to stabilize. Figure 2 shows the isotherm plotted along with the data of Reich et al. (1980). The isotherm found for the CO_2/activated carbon system is easily reproducible over the entire pressure range. Agreement with the data of Reich et al. is good.

Very low frequency data also can be used to determine the slope of the isotherm at the pressure that is being studied. The slopes of the isotherm at several different pressures can be used to construct an isotherm.

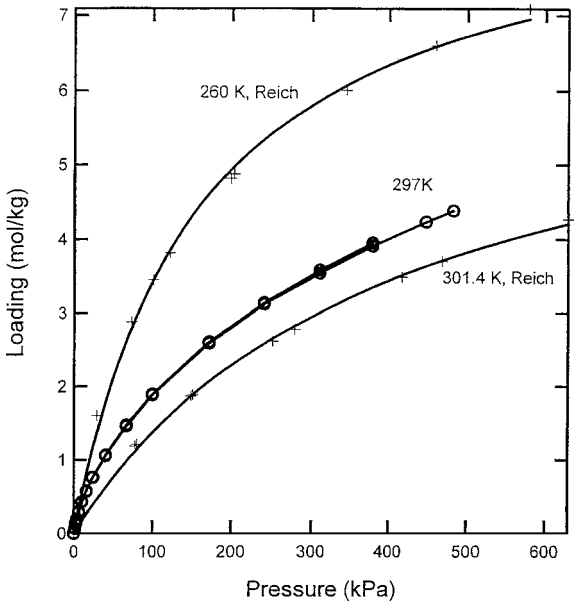

Figure 2. Isotherm of CO_2/activated carbon and the data of Reich et al. (1980).

Adsorption Dynamics Theory

Frequency response data are obtained by setting the flow rate of the gas through the system, the baseline pressure, and the sinusoidal variation of pressure about the baseline value. The mass flow rate out is recorded. After initial transient effects have subsided, a periodic pattern is reached. By comparing the response of an adsorbable gas to that of an inert gas, the adsorption-related effects can be determined for the system.

In order to extract information from the system we must generate mathematical models predicting the system response. The pressure controller is sent the sinusoidal pressure variation. In order to ensure that the actual pressure variation of the system is used, the experimental pressure data are fit to

$$P = P_o + A\sin(\omega t) \tag{2}$$

The experimental flow rate data are fit to the equation

$$F_{\text{out}} = F_o + B\sin(\omega t + \phi) \tag{3}$$

It should be noted that the flow rate variation for the system is $\pi/2$ out of phase with the pressure variation if there are no mass transfer effects in the system. When the pressure is at a maximum or a minimum, the flow rate should be passing through its midpoint. The ratio B/A is the amplitude ratio which can be plotted as a function of cycling frequency ω. ϕ is the phase angle of the system. Theoretical curves for the values of the linear driving force and surface diffusion models can be fit to amplitude ratio data to determine the LDF coefficient k or the surface (or micropore) diffusion coefficient $\mathcal{D}$ to characterize the adsorbent/adsorbate pair.

In modeling the frequency response of the system, one must consider three influences on the response of the system. First is the adsorption and desorption of the adsorbate on the sorbent. Second is the accumulation of the species in the gas phase. The third influence is the effect of pressure drops along the system and through the measurement apparatus. The portion of the system where a flow restriction becomes a factor is in the mass flow meter, located between the pressure controller and the vacuum pump. The mass flow meter contains a small diameter passage directing flow past a thermal conductivity detector.

The system is modeled as consisting of two volumes as shown in Fig. 1: first, the bed and all of the connections between the mass flow controller and the pressure

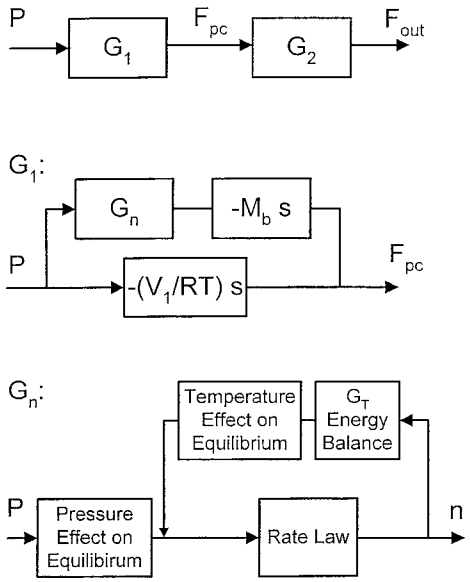

Figure 3. Block diagram describing the system model. G_2 describes the effects of the second volume. G_n describes the adsorbed phase effects.

controller, and second, the volume between the pressure controller and the mass flow meter. The flow rate out of the first volume becomes the input to the second volume.

The block diagram used to describe the system is shown in Fig. 3. G_1 and G_2 are the transfer functions for the first and second volumes, respectively. $G_{\bar{n}}$ describes the adsorbed phase effects, and $[-(V_1/RT)s]$ is the transfer function for the gas phase response, as shown below. $G_{\bar{n}}$ consists of the two parameters that affect the adsorption equilibrium, pressure and temperature, and their impact on the rate of adsorption. In the isothermal models the temperature effect loop in $G_{\bar{n}}$ is eliminated.

Five different models have been developed for the system, isothermal and non-isothermal linear driving force (or surface barrier) and surface (micropore) diffusion models, and an isothermal linear driving force model with two different pore sizes. These models are developed below. All details including some order of magnitude comparisons are contained in Sward (2001).

Material Balances

Assuming the gas phase to be ideal and the bed to have a constant loading throughout, a simple material balance can be written

$$M_b \frac{dn}{dt} + \frac{V_1}{RT}\frac{dP}{dt} - \frac{V_1 P}{RT^2}\frac{dT}{dt} = F_{\text{in}} - F_{pc}(t) \quad (4)$$

where V_1 is the volume of the entire pressure-controlled portion of the system.

To simplify the material balance, one can examine the relative sizes of the individual terms. The dn/dt and dP/dt terms are of similar magnitude. However, for the system of this work, the magnitude of the dT/dt term is comparatively small. Therefore, even in the non-isothermal models, we can neglect the dT/dt term.

We can write the following deviation variables to simplify the material balance:

$$n' = n - n_o \quad (5)$$

$$P' = P - P_o \quad (6)$$

$$T' = T - T_o \quad (7)$$

$$F'_{pc} = F_{pc} - F_{\text{in}} \quad (8)$$

Taking the material balance in Eq. (4), substituting the deviation variables, taking the Laplace transform and simplifying gives

$$M_b G_{\bar{n}} \bar{P}(s)\, s + \frac{V_1}{RT_o}\bar{P}(s)\, s = -\bar{F}_{pc}(s) \quad (9)$$

The transfer function for the first volume is

$$G_1(s) = \frac{\bar{F}_{pc}}{\bar{P}} = -M_b G_{\bar{n}} s - \frac{V_1}{RT_o}s \quad (10)$$

Using $s = j\omega$ we can write the adsorbed phase transfer function $G_{\bar{n}}(s)$ in terms of its real and imaginary parts:

$$G_{\bar{n}}(j\omega) = \text{Re}[G_{\bar{n}}(j\omega)] + j\ \text{Im}[G_{\bar{n}}(j\omega)] \quad (11)$$

Equation (11) can then be substituted into Eq. (10) and $s = j\omega$ substituted to give the expression

$$G_1(j\omega) = \omega M_b \text{Im}[G_{\bar{n}}(j\omega)] - j\omega\left\{M_b \text{Re}[G_{\bar{n}}(j\omega)] + \frac{V_1}{RT_o}\right\} \quad (12)$$

The amplitude and phase angle response of G_1 can then be determined from the real and imaginary

parts:

$$|G_1(j\omega)| = \omega\sqrt{\left(M_b\,\mathrm{Re}[G_{\bar{n}}(j\omega)] + \frac{V_1}{RT}\right)^2 + (M_b\,\mathrm{Im}[G_{\bar{n}}(j\omega)])^2} \tag{13}$$

$$\phi_1(j\omega) = \tan^{-1}\left[-\frac{M_b\,\mathrm{Re}[G_{\bar{n}}(j\omega)] + \frac{V_1}{RT}}{M_b\,\mathrm{Im}[G_{\bar{n}}(j\omega)]}\right] \tag{14}$$

A material balance on the second volume can be written

$$\frac{V_2}{RT}\frac{dP_2}{dt} = F_{pc} - F_{\mathrm{out}}(t) \tag{15}$$

Flow out of the second volume is modeled using $F_{\mathrm{out}} = \eta P_2$ where P_2 is the pressure between the pressure controller and the mass flow meter, and the pressure downstream of the mass flow meter is very small (taken to be zero). The value of η was measured experimentally and was slightly pressure dependent at low system pressures. The transfer function for the second volume is

$$G_2(s) = \frac{\bar{F}_{\mathrm{out}}}{\bar{F}_{pc}} = \frac{1}{1 + sV_2/(\eta RT)} \tag{16}$$

giving

$$|G_2(j\omega)| = \frac{1}{\sqrt{1 + \left(\frac{V_2}{\eta RT}\,\omega\right)^2}} \tag{17}$$

$$\phi_2(j\omega) = \tan^{-1}\left[-\frac{V_2}{\eta RT}\,\omega\right] \tag{18}$$

Given the values of G_1 and G_2, the overall transfer function for the apparatus can be calculated:

$$G_{\mathrm{overall}} = \frac{\bar{F}_{\mathrm{out}}}{\bar{P}} = G_1G_2 = \frac{\bar{F}_{pc}}{\bar{P}}\frac{\bar{F}_{\mathrm{out}}}{\bar{F}_{pc}} \tag{19}$$

The overall amplitude response of the system can be obtained by multiplying Eqs. (13) and (17). The phase angle can be obtained by adding Eqs. (14) and (18).

Energy Balance

Heat transfer within a packed bed is a complex issue, with energy being transferred from a particle to the wall through both the particles and the gas phase. Complex models of heat transfer allow for a radial temperature distribution with differing temperatures between the particles and the fluid (Li and Finlayson, 1977; Suzuki, 1990). There are several ways that the heat transfer model can be simplified. One simplification eliminates the temperature difference between the particle and the fluid and lumps together the heat transfer resistances through the gas and through the particles into a single parameter but maintains a radial temperature gradient within the bed. In our model, we use a further simplification in which we assume that the bed is at a uniform temperature and the heat transfer resistance is between the bed and the tubing wall. The heat transfer resistance could also be modeled between the particle and the fluid. Here the gas is assumed to be at the temperature of the tubing wall with only the temperature of the particle itself varying. This would result in a mathematically identical model with different parameter values. However, we will show experimentally that a heat transfer resistance is more than just the resistance between the particle and the fluid.

Assuming the heat transfer coefficient to be independent of temperature over the small range of variation, an energy balance can be written

$$[(n_f + n_a)\,C_p + M_bC_s]\,\frac{dT}{dt} + M_b\lambda\frac{dn}{dt} = F_{\mathrm{in}}\hat{h}_{\mathrm{in}} - F_{\mathrm{out}}\hat{h}_{\mathrm{out}} - hA[T(t) - T_{\mathrm{wall}}] \tag{20}$$

The heat capacity of the adsorbate is less than 4% of the heat capacity of the solid phase. Heat stored within the adsorbate can therefore be neglected and the $(n_f + n_a)C_p$ term can be discarded.

Since the frequency response method makes only small perturbations to the system, the adsorption equilibrium can be considered linear about the equilibrium point, giving

$$n^* = n^*(P_o, T_o) + K(P - P_o) + K_T(T - T_o) \tag{21}$$

where n^* is the amount adsorbed that is in equilibrium at pressure P and temperature T, and P_o and T_o are the equilibrium pressure and temperature about which the pressure is varied. K is the slope of the isotherm, and K_T is the slope of the isobar. K and K_T are related

through

$$\left.\frac{\partial n^*}{\partial T}\right|_P = -\left.\frac{\partial n^*}{\partial P}\right|_T \left.\frac{\partial P}{\partial T}\right|_{n^*} \tag{22}$$

which together with the Clausius-Clapeyron-type equation defining the isosteric heat of adsorption λ (taken to be negative) gives

$$K_T = -K\left(-\lambda\frac{P}{RT^2}\right) \tag{23}$$

We can linearize and simplify the energy balance to allow solution by Laplace transforms. Thus, we have

$$\hat{h}_{\text{in}} = \hat{h}_{\text{ref}} + C_p[T_o - T_{\text{ref}}] \tag{24}$$

$$\hat{h}_{\text{out}} = \hat{h}_{\text{ref}} + C_p[T(t) - T_{\text{ref}}] \tag{25}$$

Substituting into Eq. (20) and linearizing about F_{in} and T_o gives the linearized energy balance

$$M_b C_s \frac{dT}{dt} + M_b\lambda\frac{dn}{dt} = -\alpha T(t) \tag{26}$$

where $\alpha = F_{\text{in}}C_P + hA$. The Laplace transform of Eq. (26) can be rearranged, giving the energy balance transfer function

$$G_T(s) = \frac{\bar{T}}{\bar{n}} = -\frac{M_b\lambda s}{M_b C_s s + \alpha} \tag{27}$$

Linear Driving Force Models

Given Eqs. (12) and (16), all that is needed is an expression for $G_{\bar{n}}$ to predict the behavior of the system. The simplest form of kinetic model is the linear driving force (LDF) model (or surface barrier model), for which the rate of adsorption is written

$$\frac{dn}{dt} = k(n^* - n) \tag{28}$$

Isothermal Single Pore Model. Assuming that the system is isothermal, substituting the linearized isotherm into the LDF model, and writing it in terms of deviation variables gives

$$\frac{dn}{dt} = k(KP' - n') \tag{29}$$

taking the Laplace transform and solving for $G_{\bar{n}}$ gives

$$G_{\bar{n}}(s) = \frac{\bar{n}}{\bar{P}} = \frac{Kk}{s + k} \tag{30}$$

The substitution $s = j\omega$ can be made and the transfer function split into the real and imaginary parts:

$$\text{Re}[G_{\bar{n}}(j\omega)] = \frac{Kk^2}{\omega^2 + k^2} \tag{31}$$

$$\text{Im}[G_{\bar{n}}(j\omega)] = -\frac{\omega Kk}{\omega^2 + k^2} \tag{32}$$

The real and imaginary parts of $G_{\bar{n}}(j\omega)$ can be substituted into Eqs. (13) and (14) in order to calculate the amplitude ratio and phase angle of the system.

Figure 4 shows the amplitude ratio component of the frequency response for the isothermal linear driving force model for several values of the mass transfer coefficient k. The amplitude ratio is divided by frequency to eliminate the factor ω in Eq. (13). This gives greater meaning to the low frequency asymptotes. Values along the $k = 0$/s curve show just gas phase effects. Along this curve, no adsorption is taking place, and gas is only entering and exiting the system in response to changes in the pressure. The curve is flat at low frequencies and equal to the value of V_1/RT. At higher frequencies, the effects of the restriction in the mass flow meter

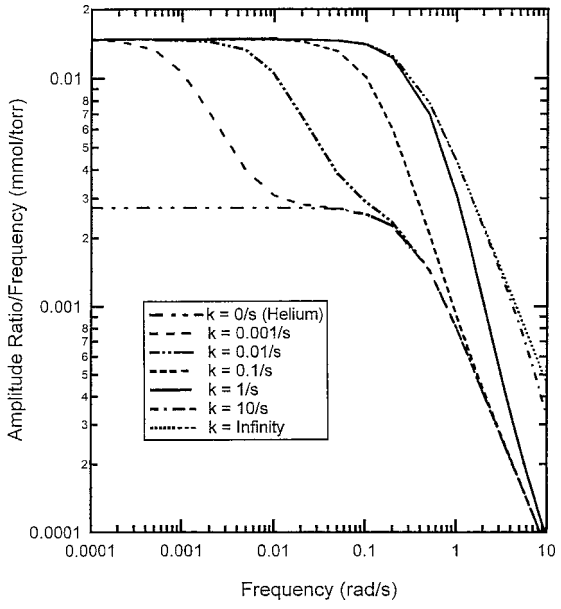

Figure 4. Sample amplitude ratio curves for isothermal linear driving force model.

attenuate the response. Along the $k = \infty$ curve, the system is at equilibrium throughout the cycle. The difference between these two curves is equal to $M_b K$. The modified curves are the equivalent of plotting the ratio of the change in number of moles in the system to the change in pressure. For the sake of brevity, this ratio (see y-axis) will be referred to as amplitude ratio throughout the remainder of the paper.

Isothermal Multiple Pore Model. We can allow for the existence of different types of pores acting in parallel within the system. We simply assume that each type of pore has a characteristic rate of adsorption. In this simple model we assume that for each of the types of pores the isotherm remains the same, just the accessibility of the pore to the adsorbate differs. This assumption could be valid, for example if there is a barrier at the entrance to the pores that restricts access to the pores. This is the means by which many carbon molecular sieves work. If there are i different sizes of pores, then we have i different rates and $2i - 1$ degrees of freedom in describing the data.

In general, if k_i is the rate of adsorption in the pore of type i and x_i is the fraction of the pores of type i, then the linear driving force rate equation for an m pore model can be written

$$\frac{dn_{\text{total}}}{dt} = \sum_{i=1}^{m} x_i k_i (n^* - n) \tag{33}$$

This gives the transfer function

$$G_{\bar{n}}(s) = K \sum_{i=1}^{m} \frac{x_i k_i}{k_i + s} \tag{34}$$

which for a single pore model reduces to Eq. (30).

The transfer function can again be split into real and imaginary parts and substituted into Eqs. (13) and 14 to determine the theoretical behavior of the system. The expressions for the real and imaginary parts of the transfer functions are

$$\text{Re}[G_{\bar{n}}(j\omega)] = K \sum \frac{x_i k_i^2}{\omega^2 + k_i^2} \tag{35}$$

$$\text{Im}[G_{\bar{n}}(j\omega)] = -K \sum \frac{\omega x_i k_i}{\omega^2 + k_i^2} \tag{36}$$

Non-Isothermal Single Pore Model. The previous two models are relatively easy to develop, as the pressure of the system is the only variable which influences the equilibrium loading of the adsorbent. Once the condition of isothermality is eliminated, the models are more complex. An increase in pressure results in an increased loading. This increase in loading liberates the heat of adsorption which raises the temperature of the adsorbent, reducing its equilibrium loading.

Taking the linearized isotherm (Eq. (21)), substituting it into Eq. (28), putting it into deviation variable form, and taking the Laplace transform gives

$$\bar{n}s = k[K\bar{P} + K_T\bar{T} - \bar{n}] \tag{37}$$

Inserting Eq. (27) into Eq. (37) and solving for the the transfer function $G_{\bar{n}}(s)$ results in

$$G_{\bar{n}}(s) = \frac{Kk}{s + \dfrac{K_T k M_b \lambda s}{M_b C_s s + \alpha} + k} \tag{38}$$

The substitution $s = j\omega$ can be made and Eq. (38) can be split into the real and imaginary parts giving

$$\text{Re}[G_{\bar{n}}(j\omega)] = \frac{Kk^2\left[\alpha + M_b^2 C_s \omega^2 (C_s + K_T\lambda)\right]}{(\alpha k - M_b C_s \omega^2)^2 + \omega^2 (k M_b C_s + \alpha + K_T k M_b \lambda)^2} \tag{39}$$

$$\text{Im}[G_{\bar{n}}(j\omega)] = \frac{-Kk\omega\left(M_b^2 C_s^2 \omega^2 + \alpha^2 + \alpha K_T k M_b \lambda\right)}{(\alpha k - M_b C_s \omega^2)^2 + \omega^2 (k M_b C_s + \alpha + K_T k M_b \lambda)^2} \tag{40}$$

Surface Diffusion Model

A model utilizing surface diffusion (or micropore diffusion) as the rate limiting step can be developed from the linearized isotherm and the material balances above and the equation for local adsorption rate. The rate law and boundary conditions for a spherical domain for diffusion are

$$\frac{\partial n}{\partial t} = \frac{\mathcal{D}}{r^2}\frac{\partial}{\partial r}\left(r^2 \frac{\partial n}{\partial r}\right) \tag{41}$$

$$n = n^* \quad \text{at} \quad r = r_p \tag{42}$$

$$\partial n/\partial r = 0 \quad \text{at} \quad r = 0 \tag{43}$$

Note that a constant diffusion coefficient has been used, which is easily justified for this linearized system. The Laplace transform of the rate law given in Eq. (41) is a

modified spherical Bessel equation of the form

$$z^2\frac{d^2\bar{n}}{dz^2} + 2z\frac{d\bar{n}}{dz} - z^2\bar{n} = 0 \tag{44}$$

where

$$z = r\sqrt{s/\mathcal{D}} \tag{45}$$

The solution is of the form

$$\bar{n} = C_1\frac{\sinh z}{z} + C_2\frac{\cosh z}{z} \tag{46}$$

Applying the boundary conditions gives

$$\bar{n} = \bar{n}^*\frac{R\sqrt{s/\mathcal{D}}}{\sinh(R\sqrt{s/\mathcal{D}})}\frac{\sinh(r\sqrt{s/\mathcal{D}})}{r\sqrt{s/\mathcal{D}}} \tag{47}$$

We can integrate over the radius R of the diffusion domian to find the average loading

$$\bar{n} = \frac{3\bar{n}^*}{R^3}\frac{R\sqrt{s/\mathcal{D}}}{\sinh(R\sqrt{s/\mathcal{D}})}\int_0^R \frac{\sinh(r\sqrt{s/\mathcal{D}})}{r\sqrt{s/\mathcal{D}}}\, r^2 dr \tag{48}$$

substituting $z = r\sqrt{s/\mathcal{D}}$ again gives

$$\bar{n} = \frac{\mathcal{D}}{R^2}\frac{1}{s}\frac{3\bar{n}^*}{\sinh(R\sqrt{s/\mathcal{D}})}\int_0^{R\sqrt{s/\mathcal{D}}} z\sinh z\, dz \tag{49}$$

Given that

$$\int_0^x z\sinh z\, dz = x\cosh x - \sinh x \tag{50}$$

we find

$$\bar{n} = \frac{\mathcal{D}}{R^2}\frac{1}{s}\frac{3\bar{n}^*}{\sinh\left(\sqrt{\frac{R^2}{\mathcal{D}}}\sqrt{s}\right)} \times\left[\sqrt{\frac{R^2}{\mathcal{D}}}\sqrt{s}\cosh\left(\sqrt{\frac{R^2}{\mathcal{D}}}\sqrt{s}\right) - \sinh\left(\sqrt{\frac{R^2}{\mathcal{D}}}\sqrt{s}\right)\right] \tag{51}$$

Further simplification gives

$$\bar{n} = 3\bar{n}^*\frac{\mathcal{D}}{R^2}\frac{1}{s}\left[\sqrt{\frac{R^2}{\mathcal{D}}}\sqrt{s}\coth\left(\sqrt{\frac{R^2}{\mathcal{D}}}\sqrt{s}\right) - 1\right] \tag{52}$$

Isothermal Model. Assuming that the system is isothermal, adsorption equilibrium is described by $n^{*'} = KP'$ giving the transfer function

$$G_{\bar{n}} = \frac{\bar{n}}{\bar{P}} = 3K\frac{\mathcal{D}}{R^2}\frac{1}{s}\left[\sqrt{\frac{R^2}{\mathcal{D}}}\sqrt{s}\coth\left(\sqrt{\frac{R^2}{\mathcal{D}}}\sqrt{s}\right) - 1\right] \tag{53}$$

Substituting $s = j\omega$ and using $\sqrt{j} = (1+j)/\sqrt{2}$ results in

$$G_{\bar{n}}(j\omega) = -3K\frac{\mathcal{D}}{R^2}\frac{j}{\omega}\left[\sqrt{\omega}\sqrt{\frac{R^2}{\mathcal{D}}}\frac{1+j}{\sqrt{2}}\coth \times\left(\sqrt{\omega}\sqrt{\frac{R^2}{\mathcal{D}}}\frac{1+j}{\sqrt{2}}\right) - 1\right] \tag{54}$$

Noting that

$$\coth(x + jy) = \frac{\sinh 2x - j\sin 2y}{\cosh 2x - \cos 2y} \tag{55}$$

and substituting results in

$$G_{\bar{n}}(j\omega) = 6K\frac{1}{\nu^2}\left[\frac{\nu}{2}(1-j)\frac{\sinh\nu - j\sin\nu}{\cosh\nu - \cos\nu} + j\right] \tag{56}$$

where

$$\nu = \sqrt{2\omega\frac{R^2}{\mathcal{D}}} \tag{57}$$

Splitting this into the real and imaginary parts gives

$$\mathrm{Re}[G_{\bar{n}}(j\omega)] = 3K\frac{1}{\nu}\frac{\sinh\nu - \sin\nu}{\cosh\nu - \cos\nu} \tag{58}$$

$$\mathrm{Im}[G_{\bar{n}}(j\omega)] = -6K\frac{1}{\nu^2}\left[\frac{\nu}{2}\frac{\sinh\nu + \sin\nu}{\cosh\nu - \cos\nu} - 1\right] \tag{59}$$

When inserted into Eq. (13) and used to generate the frequency response of the system, the isothermal surface diffusion model gives the curves shown in Fig. 5. The surface diffusion curves are flatter in shape than those for the linear driving force model shown in Fig. 4. The drop off in adsorption is more gradual as frequency increases in comparison to the LDF model. This is due to the fact that as the frequency rises, the effective depth of the pore decreases (Suzuki, 1990).

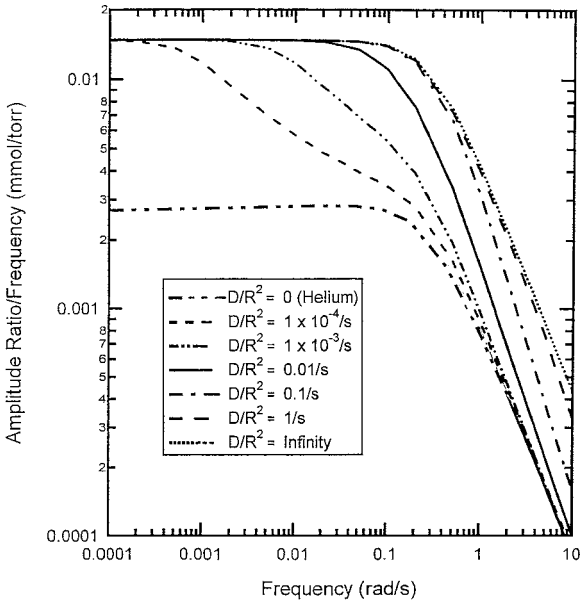

Figure 5. Sample amplitude ratio curves based for the isothermal surface diffusion model.

Non-Isothermal Model. For a non-isothermal surface diffusion model the linearized equilibrium condition $n^{*'} = KP' + K_T T'$ is applied. We again substitute Eq. (27) giving

$$\bar{n}^* = K\bar{P} - \frac{K_T M_b \lambda s}{M_b C_s s + \alpha}\bar{n} \tag{60}$$

Substituting this into Eq. (52) results in

$$\bar{n} = 3\frac{\mathcal{D}}{R^2}\frac{1}{s}\left[KP - \frac{K_T M_b \lambda s}{M_b C_s s + \alpha}\bar{n}\right] \times \left[\sqrt{\frac{R^2}{\mathcal{D}}}\sqrt{s}\coth\left(\sqrt{\frac{R^2}{\mathcal{D}}}\sqrt{s}\right) - 1\right] \tag{61}$$

Solving for $G_{\bar{n}}$, we obtain

$$G_{\bar{n}}(s) = \frac{\bar{n}}{P} = \frac{3K\frac{\mathcal{D}}{R^2}\frac{1}{s}\left[\sqrt{\frac{R^2}{\mathcal{D}}}\sqrt{s}\coth\left(\sqrt{\frac{R^2}{\mathcal{D}}}\sqrt{s}\right) - 1\right]}{1 + 3\frac{\mathcal{D}}{R^2}\frac{1}{s}\frac{K_T M_b \lambda s}{M_b C_s s + \alpha}\left[\sqrt{\frac{R^2}{\mathcal{D}}}\sqrt{s}\coth\left(\sqrt{\frac{R^2}{\mathcal{D}}}\sqrt{s}\right) - 1\right]} \tag{62}$$

Substituting $s = j\omega$ gives

$$G_{\bar{n}}(j\omega) = \frac{-3K\frac{\mathcal{D}}{R^2}\frac{j}{\omega}\left[\sqrt{\frac{R^2}{\mathcal{D}}}\sqrt{j\omega}\coth\left(\sqrt{\frac{R^2}{\mathcal{D}}}\sqrt{j\omega}\right) - 1\right]}{1 + 3\frac{\mathcal{D}}{R^2}\frac{K_T M_b \lambda}{M_b C_s j\omega + \alpha}\left[\sqrt{\frac{R^2}{\mathcal{D}}}\sqrt{j\omega}\coth\left(\sqrt{\frac{R^2}{\mathcal{D}}}\sqrt{j\omega}\right) - 1\right]} \tag{63}$$

Simplifying, we obtain

$$G_{\bar{n}}(j\omega) = \frac{-3K\frac{\mathcal{D}}{R^2}\frac{j}{\omega}\left[\sqrt{\frac{R^2}{\mathcal{D}}}\sqrt{j\omega}\coth\left(\sqrt{\frac{R^2}{\mathcal{D}}}\sqrt{j\omega}\right) - 1\right](M_b C_s j\omega + \alpha)}{(M_b C_s j\omega + \alpha) + 3\frac{\mathcal{D}}{R^2}K_T M_b \lambda\left[\sqrt{\frac{R^2}{\mathcal{D}}}\sqrt{j\omega}\coth\left(\sqrt{\frac{R^2}{\mathcal{D}}}\sqrt{j\omega}\right) - 1\right]} \tag{64}$$

Substituting $\sqrt{j} = (1 + j)/\sqrt{2}$ and using Eq. (55) gives

$$G_{\bar{n}}(j\omega) = \frac{6K\frac{1}{\nu^2}\left[\frac{\nu}{2}(1 - j)\frac{\sinh\nu - j\sin\nu}{\cosh\nu - \cos\nu} + j\right](M_b C_s j\omega + \alpha)}{(M_b C_s j\omega + \alpha) + 3\frac{\mathcal{D}}{R^2}K_T M_b \lambda\left[\frac{\nu}{2}(1 + j)\frac{\sinh\nu - j\sin\nu}{\cosh\nu - \cos\nu} - 1\right]} \tag{65}$$

Separating the numerator and denominator into real and complex parts yields

$$G_{\bar{n}}(j\omega) = \frac{6K}{\nu^2}\frac{\{\alpha\Psi^- + M_b C_s \omega\Psi^+\} + j\{M_b C_s \omega\Psi^- - \alpha\Psi^+\}}{\left\{\alpha + \beta\frac{\mathcal{D}}{R^2}\Psi^+\right\} + j\left\{M_b C_s \omega + \beta\frac{\mathcal{D}}{R^2}\Psi^-\right\}} \tag{66}$$

where

$$\beta = 3K_T M_b \lambda$$

and

$$\Psi^+ = \frac{\nu}{2}\frac{\sinh\nu + \sin\nu}{\cosh\nu - \cos\nu} - 1$$
$$\Psi^- = \frac{\nu}{2}\frac{\sinh\nu - \sin\nu}{\cosh\nu - \cos\nu} \tag{67}$$

Multiplying the numerator and denominator by the complex conjugate of the denominator and solving for

the real and imaginary parts gives

$$\mathrm{Re}[G_{\bar{n}}(j\omega)] = \frac{6K}{\nu^2} \times \frac{\{\alpha\Psi^- + M_b C_s \omega \Psi^+\}\left\{\alpha + \beta\frac{\mathcal{D}}{R^2}\Psi^+\right\} + \{M_b C_s \omega \Psi^- - \alpha\Psi^+\}\left\{M_b C_s \omega + \beta\frac{\mathcal{D}}{R^2}\Psi^-\right\}}{\left\{\alpha + \beta\frac{\mathcal{D}}{R^2}\Psi^+\right\}^2 + \left\{M_b C_s \omega + \beta\frac{\mathcal{D}}{R^2}\Psi^-\right\}^2} \tag{68}$$

$$\mathrm{Im}[G_{\bar{n}}(j\omega)] = -\frac{6K}{\nu^2} \times \frac{\{\alpha\Psi^- + M_b C_s \omega \Psi^+\}\left\{M_b C_s \omega + \beta\frac{\mathcal{D}}{R^2}\Psi^-\right\} - \{M_b C_s \omega \Psi^- - \alpha\Psi^+\}\left\{\alpha + \beta\frac{\mathcal{D}}{R^2}\Psi^+\right\}}{\left\{\alpha + \beta\frac{\mathcal{D}}{R^2}\Psi^+\right\}^2 + \left\{M_b C_s \omega + \beta\frac{\mathcal{D}}{R^2}\Psi^-\right\}^2} \tag{69}$$

Phase Angle

While the figures and examples shown have dealt with the amplitude ratio of the response, there is also information about the behavior of the system in the phase angle. Grzegorczyk and Carta (1997) showed that when particle diffusion was controlling there was a smaller phase angle shift than was present in a system with surface barrier resistance.

Characterizing the lags that are introduced by the apparatus due to forces other than adsorption is often difficult. For the frequency response apparatus, an additional phase lag is introduced by the orifice in the mass flow meter and the second volume. There may be other effects that are not apparent in the amplitude ratio response that become noticeable in the phase lag, such as the possible presence of a dead time. In order to eliminate these influences we subtract the phase angle of the inert gas at a given frequency from the phase angle of the adsorbable component at that same frequency.

Given Eqs. (14) and (18), the phase angle can be calculated giving

$$\phi = \phi_1 + \phi_2 \tag{70}$$

The value of ϕ_2, the effect of the second volume, is the same for the inert and the adsorbing gases, therefore, we have

$$\begin{aligned}\phi_{dif} &= (\phi_{1,\mathrm{ads}} + \phi_2) - (\phi_{1,\mathrm{inert}} + \phi_2) \\ &= \phi_{1,\mathrm{ads}} - \phi_{1,\mathrm{inert}}\end{aligned} \tag{71}$$

For a non-adsorbing species we can write $G_{\bar{n}} = 0$. Inserting this into Eq. (14) gives

$$\phi_{1,\mathrm{inert}} = \tan^{-1}\left[-\frac{V_1/RT}{0}\right] = \tan^{-1}(-\infty) = -\frac{\pi}{2} \tag{72}$$

The resulting expression for the phase angle difference becomes

$$\phi_{dif}(j\omega) = \tan^{-1}\left[-\frac{M_b\ \mathrm{Re}[G_{\bar{n}}(j\omega)] + \dfrac{V_1}{RT}}{M_b\ \mathrm{Im}[G_{\bar{n}}(j\omega)]}\right] + \frac{\pi}{2} \tag{73}$$

Figure 6 shows the response of the phase angle difference for the isothermal LDF model. At low frequencies the system is at equilibrium and there is no phase difference between the adsorbable and the inert response. At frequencies near the characteristic rate of adsorption, a phase lag occurs between the adsorbable and the inert systems. Then, as the frequency is increased further, the amount of adsorption decreases and the system is only showing the effects of filling and emptying the gas volume. At this point, the cycling of the adsorbable gas is fast enough to make the gas effectively inert and the difference in the phase angles disappears. This corresponds with the region on the amplitude ratio plots shown in Fig. 4 where the response curve approaches the inert gas curve.

Figure 7 plots the phase angle differences for the isothermal surface diffusion model. The surface diffusion curves have higher minima and are broader in shape than those for the linear driving force model.

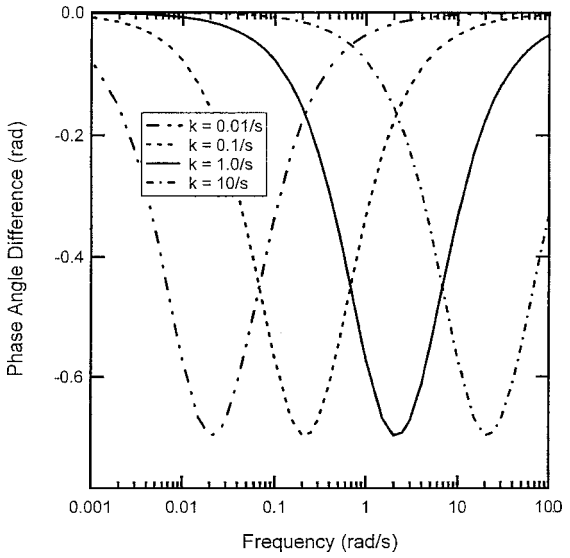

Figure 6. Phase angle differences for the isothermal LDF model for various values of the rate constant k.

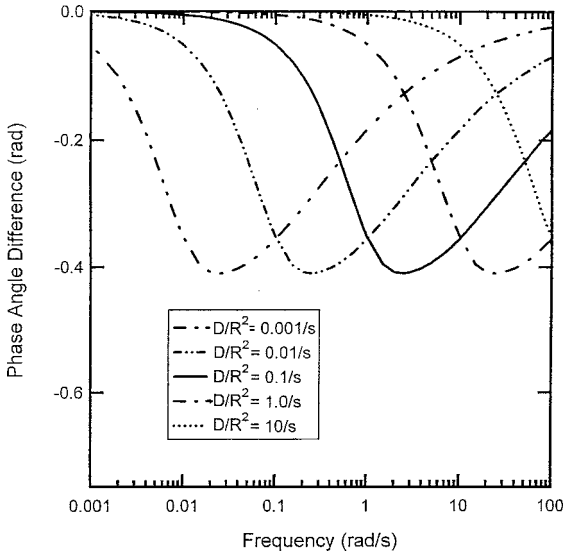

Figure 7. Phase angle differences for the isothermal surface diffusion model for various values of the rate constant $\mathcal{D}/R^2$.

Figure 8 shows how non-isothermality affects the shape of the phase angle curves. When the rate of adsorption is faster than the rate of heat dissipation the phase angle plot becomes bimodal. The phase angle change at lower frequencies occurs as the system transitions from isothermal to adiabatic operation. If the rate of adsorption is sufficiently fast there is a range of frequencies where the system is adiabatic but in equilibrium for mass exchange before the frequency becomes high enough that adsorption kinetics begin to diminish the response. Due to the heat effects on the equilibrium loadings, the maximum phase lags are smaller than those for the isothermal model.

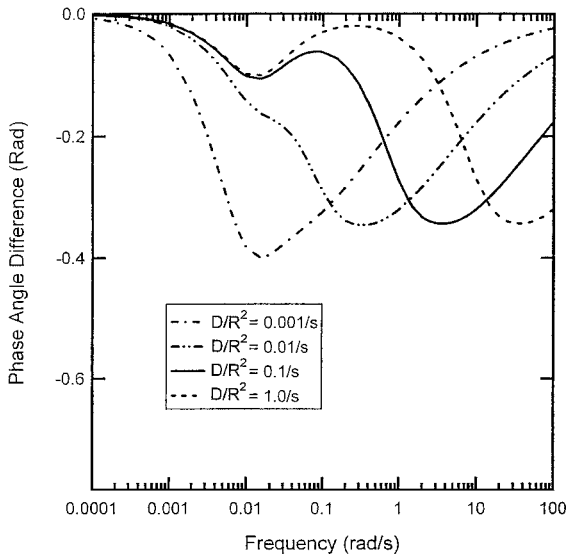

Figure 8. Phase angle differences for the non-isothermal surface diffusion model for various values of $\mathcal{D}/R^2$.

Adsorption Dynamics Experiments

In this work the system was cycled at rates from 1×10^{-4} rad/s to 8 rad/s (cycle periods of 17.5 hours to 0.8 sec). The BPL activated carbon is 6×16 mesh granular particles, approximately 3 mm in size.

Examples of measured data are shown in Fig. 9. Figure 9(a) shows sample output for amplitude and frequency of the pressure variations being 1.33 kPa (1.0 torr) and 0.1 rad/s (approximately one minute per cycle), respectively. This amplitude is only 0.5% of the total pressure. The net flow is the flow out minus the flow in. The plot of the flow rate into the system shows that the mass flow controller is able to maintain the flow rate into the system at a constant value despite the changing system pressure. From the sample output, one can see that the amplitude of the CO_2 response is greater than that of the helium. The greater amplitude exhibited by the CO_2 is due to the adsorption of the gas on the carbon. Both the CO_2 and the helium curves exhibit a small amount of phase lag. This phase lag is due to the flow restriction within the mass flow meter.

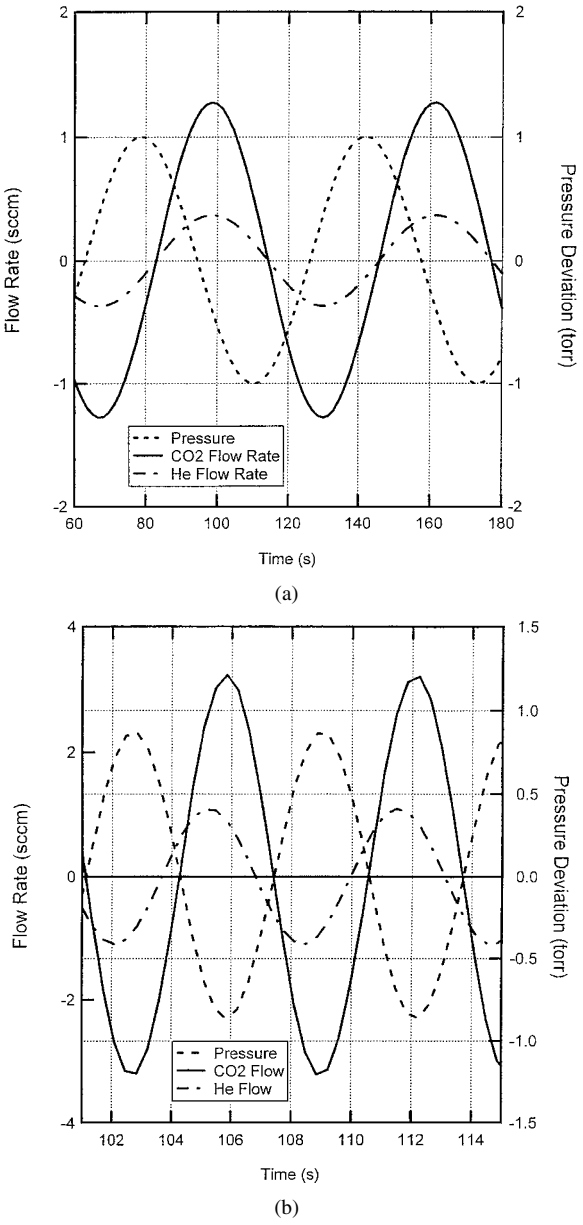

Figure 9. Example of frequency response curves at (a) 0.1 rad/s and (b) 1.0 rad/s for CO_2/BPL activated carbon.

If the flow restriction were not present, the net mass flow rates of the gases would pass through the zero line very near where the pressure curve reaches its maxima and minima. Figure 9(b) shows a second set of curves with the same parameters except a frequency of 1.0 rad/s (approximately 6 seconds per cycle). At ten times the frequency of the curves in Fig. 9(a), the effects of mass transfer resistance on adsorption are apparent. While it is difficult to see that the areas under the two curves are smaller (indicating less adsorption), the difference in phase lag is readily apparent. This difference in phase lag is due to the mass transfer resistance of the adsorbent.

One concern we had was whether there were any intraparticle fluid dynamic effects during a pressure change that would influence the rate data. Tests were run with helium and both the activated carbon and 4 mm solid glass spheres. The response of the system was the same with both materials, so it was determined that flow resistances did not play a major role in the system.

A second concern was the possible influence of pressure drops across the bed attenuating the pressure perturbation experienced by the bed. With the system bypass removed, a second pressure meter was placed upstream of the bed. The amplitude of the pressure wave showed less than 3% attenuation at a frequency of 3 rad/s. Considering that the bypass contributes to decreasing the pressure drop through the bed and all the experiments were conducted with the bypass open, the attenuation of the pressure wave by the bed can be considered negligible.

A final concern was that there were effects on the frequency response caused by different volumes of gas entering and exiting the bed. In other words, that because a greater volume of gas must enter and exit the bed in the case of the adsorbing component, that this would impact the frequency response. The amplitude of the helium pressure wave was varied over a wide range. There was no dependence of either value on the size of the pressure wave when the system was cycled at 0.5 rad/s with pressure amplitudes from 0.2 torr to 5.0 torr.

For the set of experiments, the bed was loaded with 5.37 g of BPL activated carbon. For each run, the system response was measured with helium as the working fluid. The system was then purged and the experiment was repeated with CO_2. The frequency response of the system was measured from 0.001 rad/s to 8 rad/s at a base pressure of 200 torr (26.7 kPa). The amplitude of the pressure change was between 0.2 torr (0.027 kPa) and 10 torr (1.33 kPa) depending on the frequency of oscillation. Parameter values in Table 1 were used in the determination of kinetic parameters.

In comparing experimental results with model predictions, it became quickly apparent that the single pore isothermal LDF model and the isothermal surface diffusion model could not describe the data for CO_2/BPL activated carbon adequately. However, the isothermal

Table 1. Properties used in kinetic models for carbon dioxide/activated carbon.

$M_b = 5.37$ g	$C_s = 1.088$ J/(g K)
$C_p = 0.037$ J/(mmol K)	$F_{\text{in}} = 6.0$ cm^3/min (STP)
$V_f = 50.7$ ml	$T_o = 298$ K
$K = 2.326 \times 10^{-3}$ mmol/(g Torr)	$K_T = -1.1492 \times 10^{-2}$ mmol/(g K)
$\lambda = -23$ J/mmol	

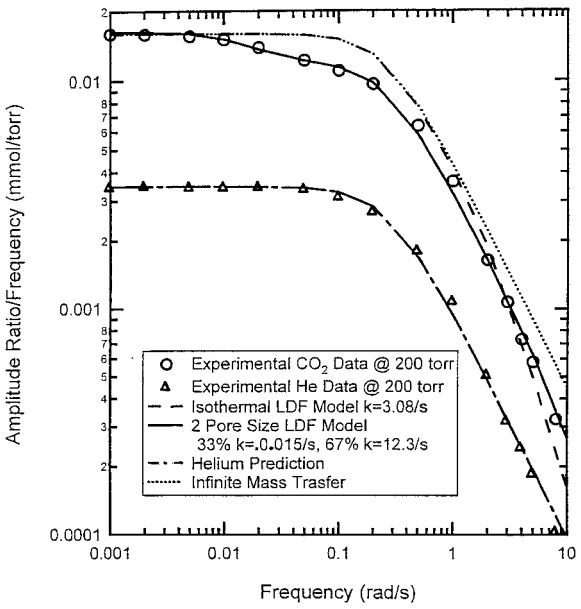

Figure 10. Plot of amplitude ratio for the two-pore isothermal LDF model for CO_2/BPL activated carbon.

multiple pore model with two pores could describe the data well, as shown in the amplitude ratio plot in Fig. 10. The best fit was determined by least squares regression of the log of the amplitude ratios. The figure also shows the experimental and theoretical curves for the system with helium. Two scales of rate behavior are shown for CO_2/BPL activated carbon in the figure, one at high frequencies and one in the range of roughly 0.01 to 0.3 rad/s. The two-pore model, with two resistances, could capture this behavior. However, the single pore isothermal LDF model and the isothermal surface diffusion model, each with a single resistance, could not.

Figure 11 shows the best fit for the non-isothermal surface diffusion and LDF models. At low frequencies, the system is very close to equilibrium; this is where it is equal to the infinite mass transfer curve. While the data breaks away from the equilibrium curve at a frequency

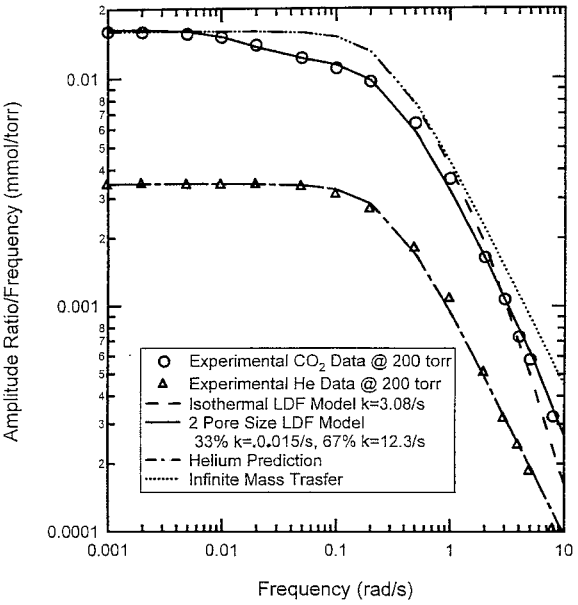

Figure 11. Plot of amplitude ratio for the non-isothermal surface diffusion and LDF models for CO_2/BPL activated carbon.

of about 0.01 rad/s, the best fit isothermal curve does not break away until a frequency of 1 rad/s, two decades later. The isothermal LDF model does not appear to fit the data well. Evidence for the non-isothermal model is supported by the calculation that if the system were completely adiabatic, the equilibrium amount adsorbed would be reduced by 1/3 (Sward, 2001). As the frequency increases the isothermal and non-isothermal model predictions approach each other. At low frequencies the times are long enough that any heat releases are allowed to dissipate. At the other end of the spectrum, as the frequency increases the loading changes become smaller, while the heat capacity of the carbon remains the same, effectively attenuating any temperature effects.

To verify that the deviations from the single pore isothermal model were due to temperature effects, the bed was packed with an equal volume mixture of carbon and stainless steel balls. The goal was to raise the heat capacity of the bed in order to attenuate any heat effects. Figure 12 shows a portion of two response curves, normalized for the amount of carbon in the bed. Over the range $\omega = 0.01$ rad/s to $\omega = 0.2$ rad/s the curve for the system with steel balls is clearly above the curve for the bed with just carbon. This is the range where the deviation from the single pore isothermal model is most evident. These results indicate that the non-isothermal

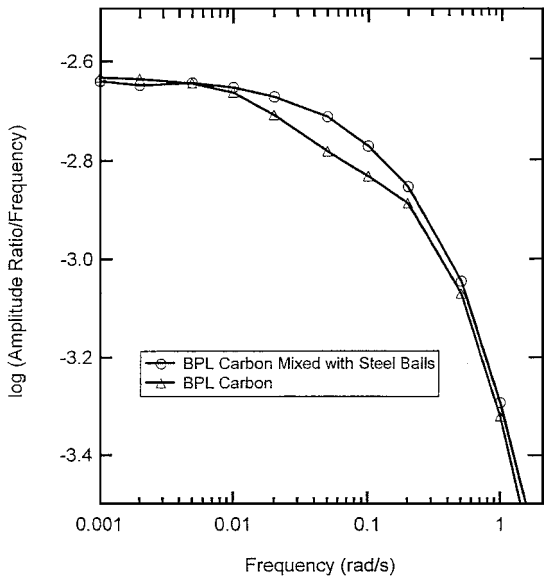

Figure 12. Amplitude response curves for CO_2/BPL activated carbon system for the bed filled with equal volumes of carbon and steel balls and carbon alone. Curves shown are straight lines connecting data points.

models are more representative of the physical reality of the system than a multiple pore model would be. In addition, since the steel balls affect the response of the system, heat transfer from the particle to the gas phase is not the only heat transfer resistance at work in the system.

The non-isothermal linear driving force model is not a perfect fit of the data at all frequencies. At the higher frequencies, the data would indicate a higher effective LDF coefficient. This can be explained by the fact that if surface diffusion within the particles is governing the mass transfer, then as the frequency increases, the apparent linear driving force coefficient increases. The depth of penetration of the adsorbate swings within the adsorbent micropores decreases with frequency. At low frequencies, the adsorbate diffuses throughout the full depth of the micropore; however, as the frequency of the pressure variation increases, the resistance to diffusion within the micropores limits adsorption and desorption to the outer portion (Suzuki, 1990). This makes the effective depth of the micropore smaller, increasing the apparent LDF constant. As was mentioned in the section on theory, the surface diffusion curves have a smaller slope than the linear driving force curves. This is a manifestation of the effects described by Suzuki.

In Fig. 11 we can see the amplitude ratio plot for the non-isothermal surface diffusion model fits the data better than the LDF model. In the case of granular activated carbon, defining the appropriate radius for the particle is difficult. The average radius of the 6×16 mesh carbon used is approximately 0.15 cm. With this value for R, the diffusivity would be $\mathcal{D} = 4.75 \times 10^{-3}$ cm^2/s.

This value is reasonable based on the apparent diffusivity of 1.56×10^{-3} cm^2/s reported by Prasetyo and Do (1998) for CO_2 at 303 K on Ajax type 976 activated carbon at very low loadings. In other work, Mugge et al. (2001) have reported a surface diffusion coefficient for carbon dioxide on Norit RB4 activated carbon of approximately 0.5×10^{-3} cm^2/s near room temperature; however, their characterization of the pore network is much different, with the resistance in mesopores and macropores and with the resistance in micropores neglected (similar to the theoretical single pore study of Taqvi and LeVan (1996)). They compare their measured values for surface diffusion coefficient of carbon dioxide, methane, and ethane with those of several other investigators for different adsorbates on different carbons finding reasonable consistency.

There is a question as to what is the appropriate radius or length scale to use in determining the value of $\mathcal{D}$. The pellet is filled with macropores and microporous domains. What needs to be determined is if the real effective radius is the average depth of a micropore in a microporous domain within the pellet, or is it the radius of the particle itself. In their work, Prasetyo and Do (1998) used similarly sized particles and used the particle diameter to calculate the diffusivity.

In order to determine whether the particle diameter impacts the rate of adsorption of carbon dioxide, particles from a sample of the activated carbon were reduced in size by grinding. It is unlikely that the micropores or microporous regions are of the same size scale as the particles. If only the micropore resistance controls the rate of adsorption, then there should be little or no change in the value of $\mathcal{D}/R^2$. The new sample of carbon had an average particle radius of 0.5 mm or one third the size of the 6×16 mesh used in the previous experiment.

A sample of 5.08 g of the new carbon was placed in the bed and frequency response measurements were made. The two sets of curves were substantially similar. For the small particles, $\mathcal{D}/R^2$ was found to be 0.53 s^{-1}. This is 1.56 times the value for the larger particles of $\mathcal{D}/R^2 = 0.34$/s. If the values of $\mathcal{D}$ are assumed to be

equal, this would indicate that the average radius of the smaller particles is 20% smaller than the radius of the larger particles. Actually, the particles are on average 67% smaller. If the particle diameter were determining distance, for the smaller particles we would the approximate diffusivity would be $\mathcal{D}/R^2 = 3.1/\text{s}$. The actual dependence of the diffusivity was $\mathcal{D} \sim R^{-0.4}$. This indicates that the main resistance is within the micropores and not the macropores of the carbon and that the size of the microporous domains is not entirely independent of particle size for 6 × 16 mesh granules.

Phase Angle Data. Based on the amplitude ratio data, the non-isothermal surface diffusion model is the best fit for the CO_2/BPL activated carbon data. In order to verify this, we can plot the phase lag of the system and compare the experimental data to the curves predicted by the various models.

Figure 13 shows the phase angle data for the CO_2/BPL system along with the curves for the linear driving force and surface diffusion models. The values for k and $\mathcal{D}/R^2$ used in the models were those that were obtained by fitting the amplitude ratio data. The phase lag data are much less uniform, especially at the higher frequencies. While it follows the general shape of the two curves, the data are scattered. Comparing the shapes of the two curves, while the phase lag at high frequencies is smaller than predicted by either model, it is closer to that predicted by the surface diffusion model. The scatter in the data is the result of the phase lag caused by the second volume. At high frequencies, the phase angle ϕ_{dif} is obtained by subtracting two numbers of similar magnitudes (see Eq. (71)).

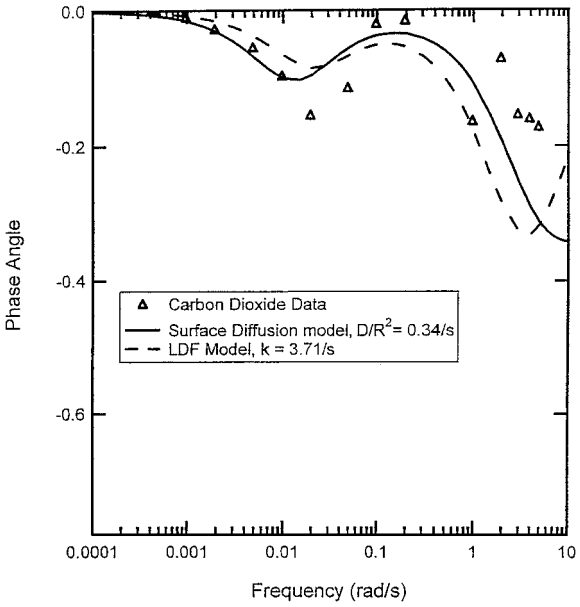

Figure 13. Phase lag of CO_2/BPL activated carbon with the phase angle predicted based on the fits of the LDF and surface diffusion models to the amplitude ratio data.

Discussion

The frequency response apparatus described can be compared with other techniques for studying adsorption kinetics. Frequency response techniques allow for easy probing of different mass transfer resistances as the frequency is changed. From the data we were able to discern the heat transfer effects that impact the rate of adsorption. Varying the frequency can also be used to separate out the effects of multiple mass transfer resistances. In addition, if a step-change approach were warranted, the apparatus is capable of creating step changes through the input of a low frequency square wave.

While the benefits mentioned above are common to all frequency response techniques, this apparatus has some positive attributes when compared with batch adsorber frequency response methods. Because the system is a flow system, heat transfer effects on adsorption are reduced, with the flowing gas attenuating some of the temperature change. Moreover, it should be easier to adapt a flow system to multicomponent adsorption studies; the exiting gas can be analyzed without concern for the impact of the sampling on the contents of the system. Also, with a flow system, any inert gas that may not have been removed from the system initially will be purged, unlike closed volumetric perturbation systems.

However, there are areas where batch systems are more capable than the current system. The current configuration is capable of operating at up to approximately 1.25 Hz. Most batch system data are reported up to approximately 10 Hz, and some are capable of operating at much higher frequencies (Shen and Rees, 1994). This is a disadvantage that might be reduced somewhat by changing the mass flow meter to reduce the flow restriction and by shortening the length of the tubing connecting the bed to the mass flow and pressure controllers to reduce the overall system volume.

The apparatus described is somewhat similar to the flow system described by Do and coworkers (Park et al., 1998; Petkovska and Do, 1998), which modulates the flow rate in and has a constant volumetric flow rate

out. For the system described in this paper, the baseline pressure of the system can be set directly.

Conclusions

A simple apparatus for the investigation of both dynamic and equilibrium characteristics of gas-phase adsorption systems has been described and demonstrated. It is capable of measuring equilibrium data for relatively fast adsorbing species at pressures of approximately 1.3 to 500 kPa or higher. It is also capable of obtaining frequency response over a frequency range of approximately five decades, with a maximum frequency of approximately 1 Hz. The apparatus holds promise as an easy to use system for the study of the dynamic behavior of gas-phase adsorption systems. It can be used for characterizing the adsorption of a variety of systems. The shape of the frequency response curves can be used to determine the controlling resistance and provide insight into the behavior of the adsorbent/adsorbate pair. Five different models of mass transfer have been developed for use with the system.

In equilibrium studies, the apparatus provided readily repeatable equilibrium data for the CO_2/activated carbon system. These values agreed well with the results obtained from the literature and the frequency response experimental data.

The system also gave repeatable results for the dynamic behavior of the CO_2/activated carbon system. For frequency response work, the system was tested to assure the linear behavior of the system to various changes of the system parameters. The values obtained for the rate parameters were reasonable given the literature values that were available. The activated carbon system was shown to follow non-isothermal surface diffusion kinetics (micropore diffusion). The magnitude of the uptake rate was found to vary with the inverse of particle size to the 0.4 power.

Nomenclature

A Amplitude of pressure change (kPa); area of bed for heat transfer (cm^2)
B Amplitude of flow rate change (mmol/s)
C_p Gas heat capacity (J/mol K)
C_s Solid heat capacity (J/g K)
$\mathcal{D}$ Effective diffusivity (cm^2/s)
F Flow rate (mmol/s)
h Heat transfer coefficient (J/cm^2 K s)
$\hat{h}$ Enthalpy (J/mol)
k Linear driving force constant (1/s)
K Slope of isotherm (mmol/g kPa)
K_T Slope of isobar (mmol/g K)
M_b Mass of bed (g)
n Adsorbed phase concentration (mmol/g)
P Pressure (mm Hg, kPa)
R Radius of spherical diffusion domain or adsorbent particle (cm; gas constant)
t Time (s)
T Temperature (K)
V Volume (cm^3)
x Weight fraction

Greek Letters

α Lumped heat transfer parameter (J/K s)
λ Heat of adsorption (J/mmol)
η Orifice coefficient for mass flow meter
ψ System phase lag (rad)
ϕ Adsorption phase lag (rad)
ω Frequency (rad/s)

Subscripts

a Adsorbed-phase
b Bed
f Gas-phase
o Equilibrium value
pc Pressure controller

Acknowledgment

The authors are grateful to the U. S. Army ECBC for financial support.

References

Alpay, E. and D.M. Scott, "The Linear Driving Force Model for Fast-Cycle Adsorption and Desorption in a Spherical Particle," *Chem. Eng. Sci.*, **47**, 499–502 (1991).

Boniface, H.A. and D.M. Ruthven, "Chromatographic Adsorption with Sinusoidal Input," *Chem. Eng. Sci.*, **40**, 2053–2061 (1985).

Bourdin, V., P.H. Grenier, F. Meunier, and L.M. Sun, "Thermal Frequency Response Method for the Study of Mass-Transfer Kinetics in Adsorbents," *AIChE J.*, **42**, 700–712 (1996).

Bülow, M. and A. Micke, "Determination of Transport Coefficients in Microporous Solids," *Adsorption*, **1**, 29–48 (1995).

Carta, G., "The Linear Driving Force Approximation for Cyclic Mass Transfer in Spherical Particles," *Chem. Eng. Sci.*, **48**, 622–625 (1992).

Do, D.D., *Adsorption Analysis: Equilibria and Kinetics*, Imperial College Press, London, 1998.

Grenier, P.H., A. Malka-Edery, and V. Bourdin, "A Temperature Frequency Response Method for Adsorption Kinetics Measurement," *Adsorption*, **5**, 135–143 (1999).

Grzegorczyk, D.S. and G. Carta, "Frequency Response of Liquid-Phase Adsorption on Polymeric Adsorbents," *Chem. Eng. Sci.*, **52**, 1589–1608 (1997).

Jordi, R.D. and D.D. Do, "Analysis of the Frequency Response Method for Sorption Kinetics in Bidispersed Structured Sorbents," *Chem. Eng. Sci.*, **48**, 1103–1130 (1993).

Jordi, R.D. and D.D. Do, "Analysis of the Frequency Response Method Applied to Non-Isothermal Sorption Studies," *Chem. Eng. Sci.*, **49**, 957–979 (1994).

Kärger, J. and D.M. Ruthven, *Diffusion in Zeolites and Other Microporous Solids*, Wiley, New York, 1992.

Li, Y., D. Willcox, and R.D. Gonzalez, "Determination of Rate Constants by the Frequency Response Method: CO on Pt/SiO_2," *AIChE J.*, **35**, 423–428 (1989).

Li, C. and B.A. Finlayson, "Heat Transfer in Packed Beds—A Reevaluation," *Chem. Eng. Sci.*, **32**, 1055–1066 (1977).

Mugge, J., H. Bosch, and T. Reith, "Measuring and Modeling Gas Adsorption Kinetics in Single Porous Particles," *Chem. Eng. Sci.*, **56**, 5351–5360 (2001).

Nakao, S. and M. Suzuki, "Mass Transfer Coefficient in Cyclic Adsorption and Desorption," *J. Chem. Eng. Japan*, **16**, 114–119 (1983).

Onyestyak, G. and L.V.C. Rees, "Frequency Response Study of Adsorbate Mobilities of Different Character in Various Commercial Adsorbents," *J. Phys. Chem. B*, **103**, 7469–7479 (1999).

Park, I.S., M. Petkovska, and D.D. Do, "Frequency Response of an Adsorber with Modulation of the Inlet Molar Flow-Rate—I. A Semi-Batch Adsorber," *Chem. Eng. Sci.*, **53**, 819–832 (1998a).

Park, I.S., M. Petkovska, and D.D. Do, "Frequency Response of an Adsorber with Modulation of the Inlet Molar Flow-Rate—II. A Continuous Flow Adsorber," *Chem. Eng. Sci.*, **53**, 833–843 (1998b).

Petkovska, M. and D.D. Do, "Nonlinear Frequency Response of Adsorption Systems: Isothermal Batch and Continuous Flow Adsorbers," *Chem. Eng. Sci.*, **53**, 3081–3097 (1998).

Petkovska, M. and D.D. Do, "Use of Higher-Order Frequency Response Functions for Identification of Nonlinear Adsorption Kinetics: Single Mechanisms under Isothermal Conditions," *Nonlin. Dynam.*, **21**, 353–376 (2000).

Polinski, L.M. and L.M. Naphtali, "A Novel Technique for Characterization of Adsorption Rates on Heterogeneous Surfaces," *J. Phys. Chem.*, **67**, 369–375 (1963).

Prasetyo, I. and D.D. Do, "Adsorption Rate of Methane and Carbon Dioxide on Activated Carbon by the Semi-Batch Constant Molar Flow Rate Method," *Chem. Eng. Sci.*, **53**, 3459–3467 (1998).

Reich, R., W.T. Ziegler, and K.A. Rogers, "Adsorption of Methane, Ethane, and Ethylene Gases and Their Binary and Ternary Mixtures and Carbon Dioxide on Activated Carbon at 212–301 K and Pressures to 35 Atmospheres," *Ind. Eng. Chem. Proc. Des. Dev.*, **19**, 336–344 (1980).

Shen, D.M. and L.V.C. Rees, "Study of Fast Diffusion in Zeolites Using a Higher Harmonic Frequency-Response Method," *J. Chem. Soc., Faraday Trans.*, **90**, 3011–3015 (1994).

Sun, L.M., F. Meunier, and J. Kärger, "On the Heat Effect in Measurements of Sorption Kinetics by the Frequency Response Method," *Chem. Eng. Sci.*, **48**, 715–722 (1993a).

Sun, L.M., F. Meunier, and P.H. Grenier, "Frequency Response for Nonisothermal Adsorption in Biporous Pellets," *Chem. Eng. Sci.*, **49**, 373–381 (1993b).

Suzuki, M. *Adsorption Engineering*, Elsevier Science Publishing Company, New York, 1990.

Sward, B.K., Ph.D. dissertation, University of Virginia, 2001.

Taqvi, S.M. and M.D. LeVan, "Role of Convection and Diffusion in a Single Pore with Adsorptive Walls," *Adsorption*, **2**, 299–309 (1996).

Van-Den-Begin, N., L.V.C. Rees, J. Caro, M. Bülow, M. Hunger, and J. Kärger, "Diffusion of Ethane in Silicalite-1 by Frequency Response, Sorption Uptake and Nuclear Magnetic Resonance Techniques," *J. Chem. Soc., Faraday Trans. I*, **85**, 1501–1509 (1989).

Yasuda, Y. and A. Yamamoto, "Zeolitic Diffusivities of Hydrocarbons by the Frequency Response Method," *J. Catal.*, **93**, 176–181 (1985).

Yasuda, Y., "Frequency Response Method for Investigation of Gas-Surface Dynamic Phenomena," *Heterogen. Chem. Rev.*, **1**, 103–124 (1994).